Available online at www.sciencedirect.com

ScienceDirect

Chinese Journal of Aeronautics 23(2010) 529-536

Chinese Journal of Aeronautics

www.elsevier.com/locate/cja

A Quadrilateral Element-based Method for Calculation of Multi-scale Temperature Field

Sun Zhigang*, Zhou Chaoxian, Gao Xiguang, Song Yingdong

College of Energy and Power Engineering, Nanjing University of Aeronautics and Astronautics, Nanjing 210016, China

Received 11 November 2009; accepted 7 June 2010

Abstract

In the analysis of functionally graded materials (FGMs), the uncoupled approach is used broadly, which is based on homogenized material property and ignores the effect of local micro-structural interaction. The higher-order theory for FGMs (HOTFGM) is a coupled approach that explicitly takes the effect of micro-structural gradation and the local interaction of the spatially variable inclusion phase into account. Based on the HOTFGM, this article presents a quadrilateral element-based method for the calculation of multi-scale temperature field (QTF). In this method, the discrete cells are quadrilateral including rectangular while the surface-averaged quantities are the primary variables which replace the coefficients employed in the temperature function. In contrast with the HOTFGM, this method improves the efficiency, eliminates the restriction of being rectangular cells and expands the solution scale. The presented results illustrate the efficiency of the QTF and its advantages in analyzing FGMs.

Keywords: functionally graded materials; higher-order theory; temperature field; multi-scale computing; quadrilateral cell

1. Introduction

Functionally graded materials (FGMs) are a new generation of composites in which the micro-structural details are spatially varied through non-uniform distribution of the reinforcement phase(s), by using reinforcement with different properties, sizes, and shapes, as well as by interchanging the roles of reinforcement the matrix phases in a continuous manner. The result is a micro-structure that produces continuously changing thermal and mechanical properties at the macroscopic or continuum level. Although the research of the FGMs began in 1980s, enormous number of researches has already been conducted and continuously need to be expanded. In the next part, an overview is provided of the different approaches employed to model the thermo-mechanical response of FGMs[1-9].

Presently, there are two approaches available to analyze the response of FGMs to thermo-mechanical loads, called coupled and uncoupled approaches[10]. In the uncoupled approach, the graded material's micro-structure is replaced by equivalent homogenized properties which are either determined by micromechanics considerations or assumed a priority. In the coupled approach, the effect of micro-structural variation and the interaction between non-uniformly distributed inclusions are explicitly taken into account in solving the governing differential equations. The method in higher-order theory for functionally graded materials (HOTFGM) is an accurate and useful method for the analysis of FGMs that accounts for the multi-scale coupling. However, it is computationally intensive and expensive when the detailed volume discretization is required to simulate realistic micro-structural details for certain types of FGMs or to capture very high thermal and stress gradients. Even though Y. Bansal and M. J. Pindera[9] developed the reformulation of HOTFGM which can decrease the size of the overall system of equations for the thermal and mechanical problems by approximately 60%[9], the function of this method in modeling micro-structure is limited since the rectangular element must be adopted.

In order to mitigate the negative impact of rectangular element mentioned above, the quadrilateral element discretization capability was incorporated into the finite-volume theory for FGMs by M. A. A. Cavalcante, et al.[11-16] recently. In contrast with the parametric mapping used by M. A. A. Cavalcante, et al., in this article, we present another approach, which

*Corresponding author. Tel.: +86-25-84892202-2506.
E-mail address: szg_mail@nuaa.edu.cn
Foundation items: National Natural Science Foundation of China (2009ZB52028, 05C52013); Ph.D. Programs Foundation of Ministry of Education of China (20070287039)

doi: 10.1016/S1000-9361(09)60251-X

directly extends the HOTFGM to enabling the use of quadrilateral elements. Since the use of quadrangular element, we named the method developed here as quadrilateral element-based method for the calculation of multi-scale temperature field (QTF). In the QTF, a discretization based on quadrangular elements is employed to capture the graded material's heterogeneous micro-structure. The thermal field within each cell are depicted with quadratic polynomial within local coordinate system, and the unknown coefficients associated with the variables with different orders are obtained by satisfying the field equations in a surface-averaged sense for each cell, followed by the application of continuity conditions within each cell, and between adjacent cells, in a surface-averaged sense together with the imposed boundary conditions[11]. Although the parametric formulation developed by M. A. A. Cavalcante, et al.[11-13] and QTF incorporate quadrilateral element discretization capability into the HOTFGM, they have different manners of constructing the stiffness matrix of an element. In fact, the key problems in developing HOTFGM include 1) how to perform the integration of the quadrilateral elements and 2) how to integrate the stiffness matrix of each element into the global equation system. In the parametric formulation, the integration is performed by a parametric mapping of coordinate system from a reference square element to a quadrilateral element. However, in QTF, the integration is performed by a direct approach, which is described in this article. Except this difference, both methods employ global/local numbering system to establish the global equation system.

2. Theory and Formulations

The geometric model on which the QTF is based is shown in Fig.1. The cross section of the micro-structure length of the heterogeneous composite, having infinite length in the *z*-direction and being functionally graded in the *x*-*y* plane, is appropriately discretized into totally N_e elements with identical material properties and local coordinates of $x_{min} \le x \le x_{max}$ and $y_{min} \le y \le y_{max}$. The loads including a prescribed surface temperature and/or heat distribution, are applied to the *x*-*y* plane.

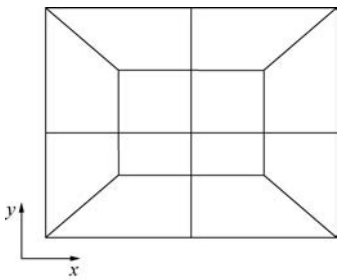

Fig.1 Discretization of QTF.

The formula of temperature within each cell employed by QTF is similar to the formula employed by HOTFGM (which is based on the quadratic polynomial in the local coordinate system attached to a cell's center), the similar manner of satisfying the governing field equations (steady-state heat conduction equation and equilibrium equation) in a surface sense, and the interfacial continuity and boundary condition in a surface-integral sense. The major difference between the QTF and the reformulated HOTFGM is in the shape of cell. Cells in the reformulation of the HOTFGM are rectangular which is shown in Fig.2 and those for the QTF are quadrilateral as shown in Fig.1.

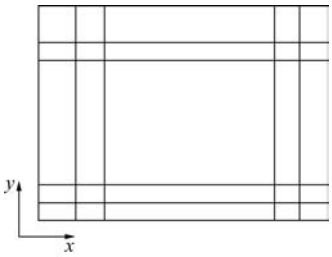

Fig.2 Discretization of reformation of HOTFGM.

Like the reformulation of the HOTFGM, the QTF should construct a local conductivity matrix that relates the surface-averaged heat flux to the surface-averaged temperature for a certain cell *i*, to satisfy the steady-state heat conduction equation[2,4].

We use the local conductivity matrices to construct the global conductivity matrix by enforcing the heat flux and temperature continuity conditions at the interfaces of the adjacent cells in an average sense. Therefore the QTF has the same efficiency as that of reformulated HOTFGM, and has larger range of application, because the reformation of the HOTFGM is based on the rectangular cells while the QTF is employing the quadrilateral elements. In mathematics, the integral method and difficulty with regard to the rectangle and the quadrangle are different, with the latter more complex than the former. For example, the global conductivity matrix of the QTF is a 4×4 matrix and each element of the matrix is a multinomial containing at least 680 elements. Compared with the QTF, the reformation of the HOTFGM is straightforward. The detailed derivations of the local and global conductivity matrices are outlined next.

2.1. Formulation of local temperature

The temperature field $T^{(i)}$ within the cell *i* is approximatly depicted by a second-order polynomial in terms of local coordinate system $x^{(i)}$, $y^{(i)}$ as

$$T^{(i)} = T^{(i)}_{(00)} + T^{(i)}_{(10)} \cdot \bar{x}^{(i)} + T^{(i)}_{(01)} \cdot \bar{y}^{(i)} + T^{(i)}_{(20)} \cdot (\bar{x}^{(i)})^2 + T^{(i)}_{(02)} \cdot (\bar{y}^{(i)})^2 \quad (1)$$

where $T^{(i)}_{(mn)}$ $(m,n=0,1,2)$ is the unknown variable associated with each cell.

The heat flux $q^{(i)}_x$ and $q^{(i)}_y$ at any point within cell *i* can be obtained from the Fourier law of heat conduction,

$$\left.\begin{aligned} q_x^{(i)} &= -k_x^{(i)} \frac{\partial T^{(i)}}{\partial \bar{x}^{(i)}} \\ q_y^{(i)} &= -k_y^{(i)} \frac{\partial T^{(i)}}{\partial \bar{y}^{(i)}} \end{aligned}\right\} \tag{2}$$

where $k_x^{(i)}$ and $k_y^{(i)}$ are the heat conductivity coefficients of the material of cell *i*, which are constant within the cell *i* in this article. Therefore the heat flux $q_x^{(i)}$ and $q_y^{(i)}$ at any point within cell *i* can be expressed as

$$\left.\begin{aligned} q_x^{(i)} &= -k_x^{(i)} \left(T_{(10)}^{(i)} + 2\bar{x}^{(i)} T_{(20)}^{(i)} \right) \\ q_y^{(i)} &= -k_y^{(i)} \left(T_{(01)}^{(i)} + 2\bar{y}^{(i)} T_{(02)}^{(i)} \right) \end{aligned}\right\} \tag{3}$$

2.2. Local conductivity matrix

The local conductivity matrix is used to find the connection between the surface-averaged temperature and the surface-averaged heat flux in one element. Compared to local conductivity matrices in the reformation of the HOTFGM, there are differences between the two kinds of local conductivity matrices. First of all, in the rectangular element, the four edges can be expressed as the top, bottom, left and right edges while in the QTF, because of the randomness of edge direction, the edges of each quadrilateral element have to be expressed with their numbering such as the 1st, 2nd, 3rd and 4th edges. Secondly, the integration in the rectangular element is comparatively simple, but the integration in the quadrilateral element has to employ local coordinate system before the integration can be carried out.

Therefore, we should find local coordinate system to obtain the expression for the surface-averaged temperature. There are several concepts used in the local coordinate implementation, including the direction vector of each edge and the length of each edge.

The first step is to construct the direction vectors ${}^{x}t_a^{(i)}$ and ${}^{y}t_a^{(i)}$ (a=1,2,3,4) and the characteristic parameters of the cells including $l_a^{(i)}$ as shown in Fig.3. The direction vectors express the unit vectors in the direction of being parallel and normal to the edges, which are defined by Eqs.(4)-(5):

$${}^{x}t_a^{(i)} = \frac{x_b^{(i)} - x_a^{(i)}}{l_a^{(i)}}, \quad {}^{y}t_a^{(i)} = \frac{y_b^{(i)} - y_a^{(i)}}{l_a^{(i)}}$$
$$(a = 1,2,3,4;\ b = 2,3,4,1) \tag{4}$$

$$l_a^{(i)} = \sqrt{\left(x_b^{(i)} - x_a^{(i)}\right)^2 + \left(y_b^{(i)} - y_a^{(i)}\right)^2}$$
$$(a = 1,2,3,4;\ b = 2,3,4,1) \tag{5}$$

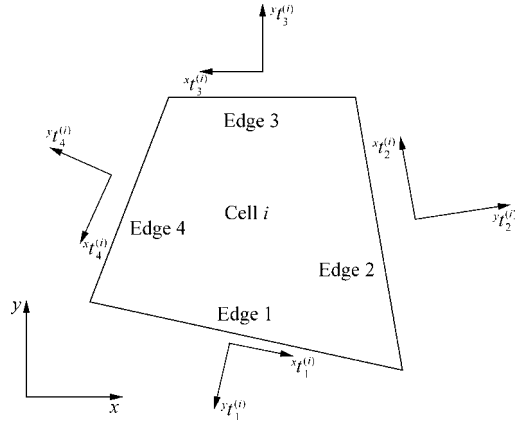

Fig.3 Direction vectors of cell *i*.

So the heat flux at the boundaries of cell can be expressed with the direction vectors.

$$q_j^{(i)} = q_x^{(i)} \cdot {}^{x}t_j^{(i)} - q_y^{(i)} \cdot {}^{y}t_j^{(i)} \qquad (j = 1,2,3,4) \tag{6}$$

The local conductivity matrix should relate the surface-averaged heat flux explicitly to the surfaced-averaged temperature. Therefore the surface-averaged heat flux $\overline{\boldsymbol{Q}}^{(i)}$ is defined at the outer boundary of the cell in the following manner (as shown in Fig.4):

$$\overline{\boldsymbol{Q}}^{(i)} = \left[\overline{Q}_1^{(i)} \quad \overline{Q}_2^{(i)} \quad \overline{Q}_3^{(i)} \quad \overline{Q}_4^{(i)} \right] \tag{7}$$

where $\overline{Q}_j^{(i)}$ (j =1,2,3,4) is defined as

$$\overline{Q}_j^{(i)} = \frac{1}{l_j^{(i)}} \int_0^{l_1^{(i)}} q_j^{(i)} \mathrm{d}l^{(i)} \tag{8}$$

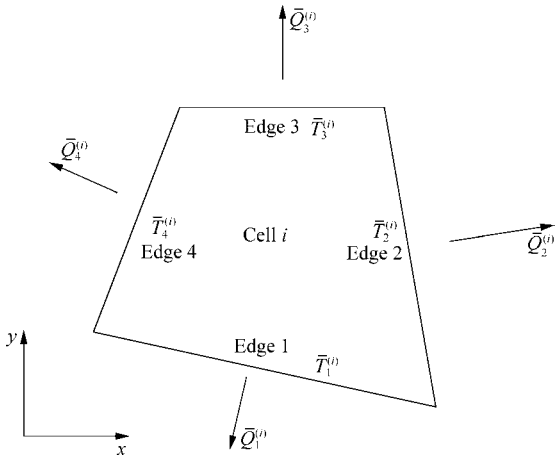

Fig.4 Surface-averaged temperature and heat flux of cell *i*.

These equations result in a matrix which relates the surface-averaged heat flux to the $T_{(mn)}^{(i)}$:

$$\left[\overline{Q}_1^{(i)} \quad \overline{Q}_2^{(i)} \quad \overline{Q}_3^{(i)} \quad \overline{Q}_4^{(i)} \right]^{\mathrm{T}} =$$
$$\boldsymbol{C}^{(i)} \left[T_{(00)}^{(i)} \quad T_{(10)}^{(i)} \quad T_{(01)}^{(i)} \quad T_{(20)}^{(i)} \quad T_{(02)}^{(i)} \right]^{\mathrm{T}} \tag{9}$$

We can get the variables through the surface-averaged temperatures $\overline{\boldsymbol{T}}^{(i)}$:

$$\bar{\boldsymbol{T}}^{(i)}=\left[\bar{T}_1^{(i)}\quad \bar{T}_2^{(i)}\quad \bar{T}_3^{(i)}\quad \bar{T}_4^{(i)}\right] \tag{10}$$

where

$$\bar{T}_j^{(i)}=\frac{1}{l_j}\int_0^{l_j}T_j^{(i)}\mathrm{d}l^{(i)}\qquad (j=1,2,3,4) \tag{11}$$

Substituting the expression of $\bar{\boldsymbol{T}}^{(i)}$ given by Eq.(1) into the preceding definitions and performing the averaging procedure, we obtain a matrix relating the surface-averaged temperature to the zeroth-, the first- and the second-order micro-variables. However, there are five unknown coefficients with four equations. In order to express these five micro-variables solely in terms of the surface-averaged temperature, we employ the steady-state heat conduction equation (Eq.(12)), which is satisfied in area sense within the cell *i*.

$$\frac{\partial q_x^{(i)}}{\partial x^{(i)}}+\frac{\partial q_y^{(i)}}{\partial y^{(i)}}=0 \tag{12}$$

Substituting Eq.(2) into Eq.(1), in conjunction with Eq.(11) and Eq.(12), we can simplify the obtained equation as follows:

$$\left[T_1^{(i)}\quad T_2^{(i)}\quad T_3^{(i)}\quad T_4^{(i)}\quad 0\right]^{\mathrm{T}}=$$
$$\boldsymbol{A}^{(i)}\left[T_{(00)}^{(i)}\quad T_{(10)}^{(i)}\quad T_{(01)}^{(i)}\quad T_{(20)}^{(i)}\quad T_{(02)}^{(i)}\right]^{\mathrm{T}} \tag{13}$$

which relates the surface-averaged temperature to the micro-variables. To obtain the inverse matrix of $\boldsymbol{A}^{(i)}$, the micro-variables can be expressed with the surface-averaged tempertures:

$$\left[T_{(00)}^{(i)}\quad T_{(10)}^{(i)}\quad T_{(01)}^{(i)}\quad T_{(20)}^{(i)}\quad T_{(02)}^{(i)}\right]^{\mathrm{T}}=$$
$$\boldsymbol{B}^{(i)}\left[T_1^{(i)}\quad T_2^{(i)}\quad T_3^{(i)}\quad T_4^{(i)}\right]^{\mathrm{T}} \tag{14}$$

Therefore, we substitute Eq.(14) into the Eq.(9), the new matrix which relates the surface-averaged temperature to the surface-averaged heat flux is obtained as follows:

$$\left[Q_1^{(i)}\quad Q_2^{(i)}\quad Q_3^{(i)}\quad Q_4^{(i)}\right]^{\mathrm{T}}=$$
$$\boldsymbol{D}^{(i)}\left[T_1^{(i)}\quad T_2^{(i)}\quad T_3^{(i)}\quad T_4^{(i)}\right]^{\mathrm{T}} \tag{15}$$

where the matrix $\boldsymbol{D}^{(i)}$ is the local conductivity matrix of the cell *i*.

According to a rough estimation, the local conductivity matrix of the cell *i* contains 16 elements, each of which is a multinomial containing at least 680 elements.

2.3. Global conductivity matrix

This step assembles the local conductivity matrices of all cells to form a global conductivity matrix, which reflects the entire thermal response of the material. To solve the global conductivity matrix, the interfacial temperature and heat flux continuity conditions and the boundary conditions should be used in the equations.

The temperature continuity conditions at the interfaces between adjacent cells are applied in an average sense.

Taking the model in Fig.5 as an example, the surface-averaged temperature at the interface between cell 1 and cell 2 should be continuous. In other words, the surface-averaged temperatures of edge 2 and edge 4 must be equal to each other, and we can express it as follows:

$$\bar{T}_2^{(1)}=\bar{T}_4^{(2)} \tag{16}$$

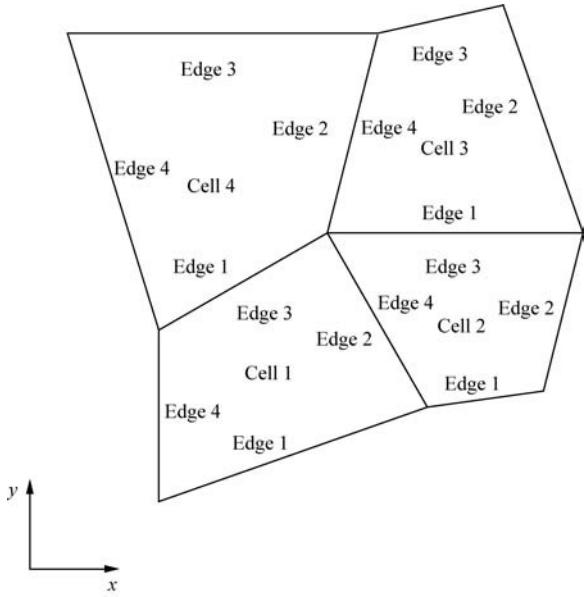

Fig.5 Continuity conditions of adjacent cells.

Similarly, considering cell 2 and cell 3, the temperature continuity at the interfaces between adjacent cells can be applied in an average sense:

$$\bar{T}_3^{(2)}=\bar{T}_1^{(3)} \tag{17}$$

There are also surface-averaged temperature at the external boundary of composite, which can be used as the boundary condition.

The heat flux continuity at the interfaces between adjacent cells is also applied in an average sense. Taking the model in Fig.5 as example, the surface-averaged heat flux at the interface between cell 1 and cell 2 should be continuous. In other words, the surface-averaged heat flux of edge 2 and edge 4 must be equal to each other, and we can express it as follows:

$$\bar{Q}_2^{(1)}-\bar{Q}_4^{(2)}=0 \tag{18}$$

where $\bar{Q}_2^{(1)}$ is the surface-averaged heat flux going out of the 2nd boundary of cell 1, and $\bar{Q}_4^{(2)}$ the surface-averaged heat flux going out of the 4th boundary of cell 2.

Similarly, considering cell 2 and cell 3, the temperature continuity at the interfaces between adjacent cells can be applied in an average sense:

$$\bar{Q}_3^{(2)}-\bar{Q}_1^{(3)}=0 \tag{19}$$

There are also surface-averaged heat flux at the external boundary of composite, which can be used as the boundary condition.

After applying the continuity conditions, the external boundary conditions should be applied. The quantity of the external boundary depends on whether the temperature or heat flux is applied on the external boundary.

For the heat transfer, there are three kinds of boundary conditions. The first boundary condition is to give the temperatures of the boundary, the 2nd boundary condition is to give the density of heat flux of the boundary, and the 3rd boundary condition is to give the surface heat transfer coefficient h between the boundary and the liquid and the temperature of the surrounding liquid t_f.

These give rise to the additional equations to solve the global conductivity matrix.

Using the local conductivity matrix of Eq.(15), the temperature continuity conditions of Eqs.(16)-(17), the surface-averaged temperatures at the boundaries, the heat flux continuity condition, Eqs.(18)-(19), and the external boundary condition, the global conductivity matrix can be expressed as the following simple form:

$$\boldsymbol{\kappa}\cdot\overline{\boldsymbol{T}}=\overline{\boldsymbol{Q}} \tag{20}$$

where $\boldsymbol{\kappa}$ is the global thermal conductivity matrix obtained through assembling the local conductivity matrices of Eq.(15), using the local/global conductivity matrices approaches explained earlier. This matrix contains the information on the geometry and thermal conductivities of the individual cells. Because of the huge scale of the global conductivity matrix, the matrix $\boldsymbol{\kappa}$ is not displayed in detail here.

The vector $\overline{\boldsymbol{T}}$ contains the unknown surface-averaged temperatures at the cell interfaces and the outer boundary of the composite (some of which are known), and is given by

$$\overline{\boldsymbol{T}}=[\overline{T}_1^{(1)}\quad \overline{T}_1^{(2)}\quad \cdots\quad \overline{T}_1^{(i)}\quad \overline{T}_2^{(i)}\quad \overline{T}_3^{(i)}\quad \overline{T}_4^{(i)}\quad \overline{T}_4^{(i+1)}\quad \cdots\quad \overline{T}_4^{(N_e)}] \tag{21}$$

And the $\overline{\boldsymbol{Q}}$ in Eq.(20) can be expressed as

$$\overline{\boldsymbol{Q}}=[\overline{Q}_1^{(1)}\quad \overline{Q}_1^{(2)}\quad \cdots\quad \overline{Q}_1^{(i)}\quad \overline{Q}_2^{(i)}\quad \overline{Q}_3^{(i)}\quad \overline{Q}_4^{(i)}\quad \overline{Q}_4^{(i+1)}\quad \cdots\quad \overline{Q}_4^{(N_e)}] \tag{22}$$

Solving the global conductivity matrix, the vector $\overline{\boldsymbol{T}}$ can be obtained, which contains all the surface-averaged temperatures at the interfaces of the cells. Substituting the expression of $\overline{T}_j^{(i)}$ into Eq.(14), the micro-variables of each cell can be obtained. Finally, the temperature field at local level can be calculated by Eq.(1).

3. Numerical Examples

3.1. Example 1

In many practical applications, multi-layers structures are widely used. In order to prevent yielding due to exposure to high temperature, certain layers are set being subjected to very high thermal gradient to protect the other layers. Here, we demonstrate the efficiency of the extended version by considering a 6-layer structure with discretized realistic micro-structure.

The geometry and the boundary conditions of the illustrated structure are shown in Figs.6-7. In Fig.6, K_x and K_y are coefficients of heat conduction in the x- and y-direction. In the y-direction of the x-y plane, the largest width is 3.2 m while the narrowest width is 2.4 m, and each of the space in the x-direction is 1 m. It is discretized into six cells. From left to right, the ratios between the six heat conductivity coefficients are 14∶150∶14∶80∶8∶60 W/(m·K), while the heat conductivity coefficients in the x-direction and in the y-direction are equivalent. The structure is subjected to 300 K at the left boundary and 100 K at the right boundary, while the bottom boundary and the top boundary are insulated from heat conduction (zero heat flux). The detailed boundary conditions are shown in Fig.7.

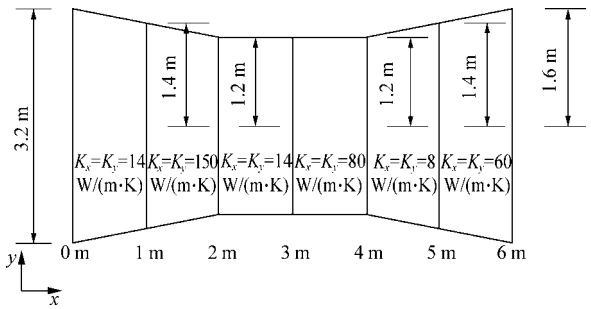

Fig.6 Detailed shape of structure.

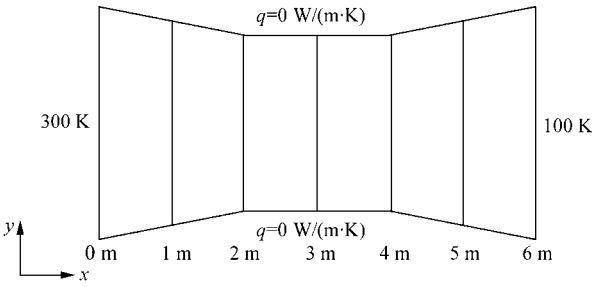

Fig.7 Heat loading sketch.

For the given geometry, micro-structure, and boundary conditions, the temperature field can be fixed using the QTF and the results should be compared with the finite-element solution. The finite-element solution can be obtained with the available tool finite-element method (FEM) to generate the same mesh and micro-structure as the QTF and carry out temperature analysis. For the finite-element solution, temperature analysis is carried out using two-dimensional and 8-noded thermal (plane 77) elements. The boundary conditions are shown in Fig.7.

In order to compare the results obtained from the

two approaches on a common basis, the nodal temperatures obtained from the FEM are exported into the same post-process as in the QTF. The temperature field generated by the QTF is essentially indistinguishable from that generated by FEM. This is seen in the cross-sectional plots for the temperature (Figs.8-9) and the horizontal numerical value (Fig.10) given that $y = 0$. In Figs.8-10, T reprensts temperature.

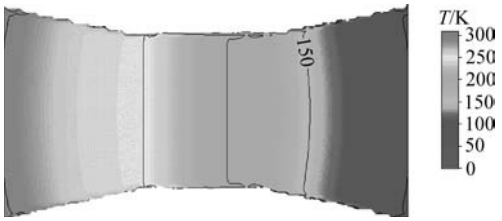

Fig.8 Temperature field obtained from QTF.

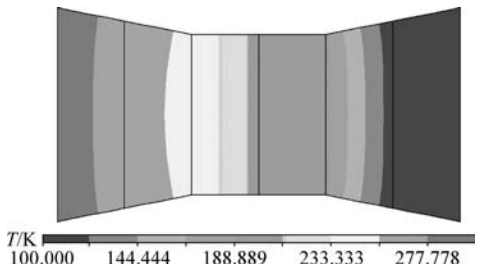

Fig.9 Temperature field obtained from FEM.

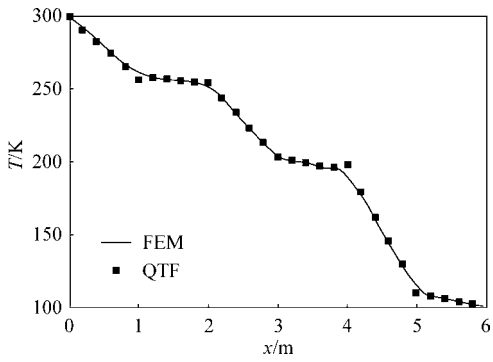

Fig.10 Horizontal numerical value given that y=0.

In Fig.10, the difference between QTF and FEM can be negligible, so for the accuracy of the temperature, the QTF is equivalent to the FEM.

3.2. Example 2

In this numerical example, there is a right angle plane, its geometry and boundary conditions are shown in Figs.11-12. In the y-direction of the x-y plane, the largest width is 4 m while the narrowest width is 2 m, and the same geometry is for the x-direction. The structure has the uniform heat conductivity coefficient: the heat conductivity coefficients in both the x-direction and y-direction are all 10 W/(m·K). The structure is subjected to 0 K at the left and the bottom boundaries, and the top face and the right boundaries are 100 K while the two northeast boundaries are 200 K. The detailed boundary condition is shown in Fig.12.

In particular, this structure is analyzed using the QTF and the results are compared and contrasted with that of FEM. For the given geometry, micro-structure, and boundary conditions, the temperature field can be fixed using the QTF and the results should be compared with the finite-element solution.

In the QTF, there are three kinds of mesh discretization, which are shown in Fig.13. The plane is meshed into 16, 24 and 80 elements, while Fig.14 shows the corresponding equivalent stress field for each mesh. The numbers in bracket are coordinates of the nodes.

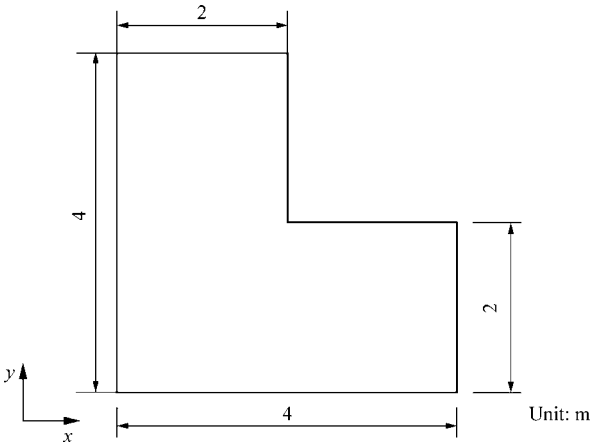

Fig.11 Detailed shape of right angle structure.

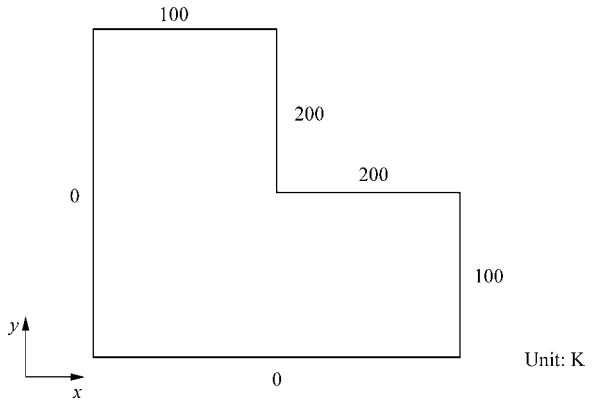

Fig.12 Loading sketch.

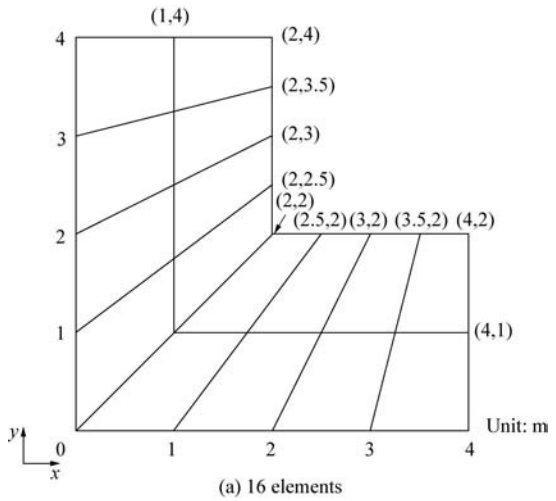

(a) 16 elements

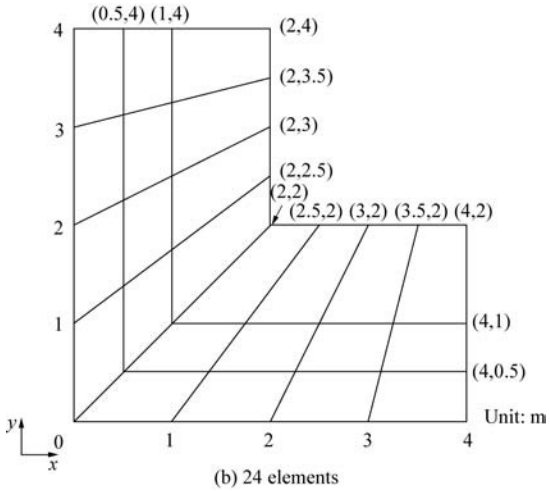

(b) 24 elements

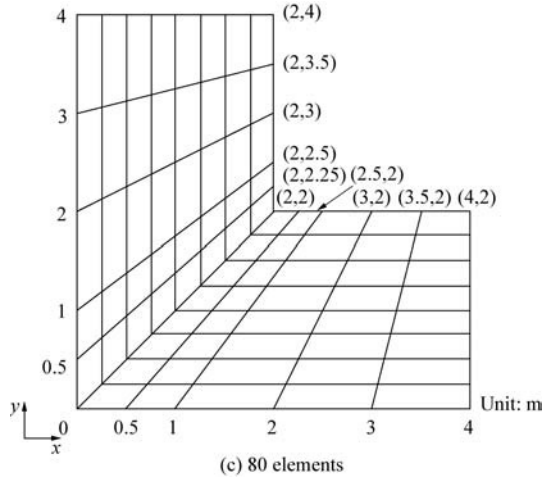

(c) 80 elements

Fig.13 Three kinds of mesh.

The finite-element solution can be obtained using the commercial FEM software with which the same mesh is generated and micro-structure and the temperature analysis are carried out. For the finite-element solution, thermal analysis is carried out using twodimensional and eight-noded thermal elements. The boundary conditions are applied as shown in Fig.12, and the result is shown in Fig.15.

From Figs.13-14, the result of the structure with 16

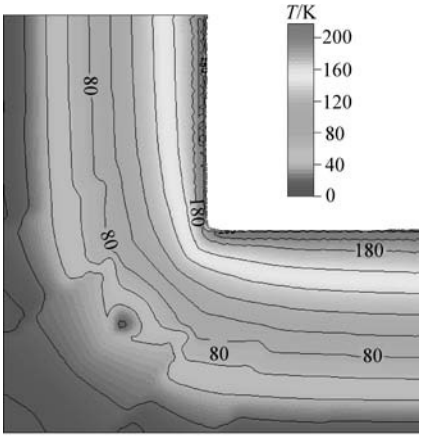

(a) 16 elements

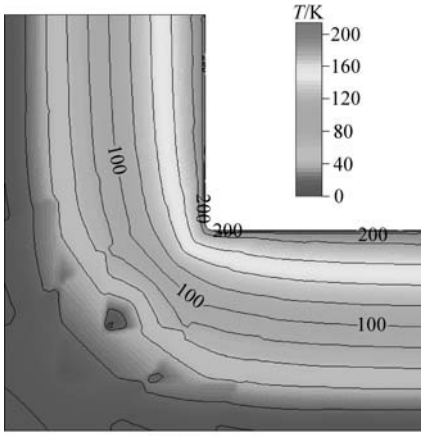

(b) 24 elements

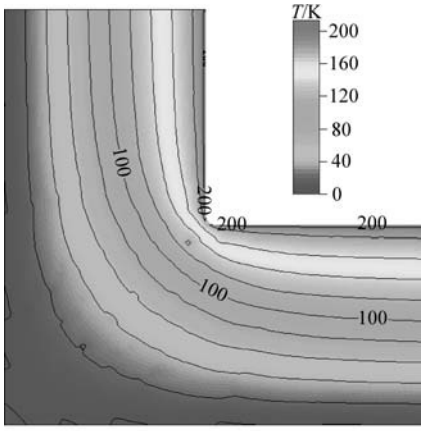

(c) 80 elements

Fig.14 Corresponding equivalent stress field.

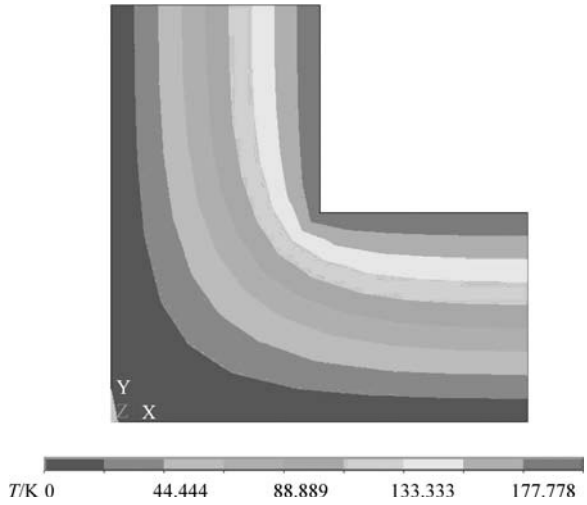

Fig.15 Result of FEM.

elements is not good and there are some discontinuous temperature points. Compared with the first kind of mesh, the temperature field of the structure with 24 elements is close to that obtained from the FEM, and the temperature discontinuity has been eliminated. When the structure is meshed by 80 elements, the temperature field is smooth and consistent with the result of the FEM.

4. Conclusions

Based on the high-order theory for FGMs, the authors develop a multi-scale method for two-dimensional temperature estimation which can use quadrilateral elements. This article puts forward the theory frame, derives the relational formulae, and at the same time eliminates the redundant continuity equations and decreases the size of the overall numbers of equations through the reformulation of the HOTFGM. In other words, the QTF expands the solution area and enhances the calculation efficiency. After being compared with the FEM, the validity of the QTF is proved.

References

[1] Muliana A H. A micromechanical model for predicting thermal properties and thermo-viscoelastic responses of functionally graded materials. International Journal of Solids and Structures 2009; 46(9): 1911-1924.

[2] Pindera M J, Arnold S M, Aboudi J, et al. Use of composites in functionally graded materials. Composites Engineering 1994; 4 (1): 1-18.

[3] Aboudi J, Pindera M J, Arnold S M. A coupled higher theory for functionally graded composites with partial homogenization. Composites Engineering 1995; 5(7): 771-792.

[4] Aboudi J, Pindera M J, Glaeser A M, et al. Use of composite in multi-phased and functionally graded materials. Composites Part B 1997; 28(1-2): 1-175.

[5] Needleman A, Suresh S. Mechanics and physics of layered and graded materials. Journal of Mechanics and Physics of Solids 1996; 44(5): 647-821.

[6] Shiota I, Miyamoto Y. Functionally graded materials. Proceedings of the 4th International Symposium on Functionally Graded Materials. Amsterdam: Elsevier, 1996; 114-121.

[7] Suresh S, Mortensen A. Fundamentals of functionally graded materials. 2nd ed. Cambridge: Cambridge University Press, 1998.

[8] Paulino G H. Fracture of functionally graded materials. Engineering Fracture Mechanics 2002; 69(14-16): 1519-1812.

[9] Bansal Y, Pindera M J. Efficient reformulation of the thermoelastic higher-order theory for functionally graded materials. Journal of Thermal Stresses 2003; 26(11-12): 1055-1092.

[10] Pindera M J, Aboudi J, Arnold S M. Limitations of the uncoupled, RVE-based micromechanical approach in the analysis of functionally graded composites. Mechanics of Materials 1995; 20(1): 77-94.

[11] Cavalcante M A A, Marques S P C, Pindera M J. Parametric formulation of the finite-volume theory for functionally graded materials Part I: analysis. Journal of Applied Mechanics 2007; 74(5): 935-945.

[12] Cavalcante M A A, Marques S P C, Pindera M J. Computational aspects of the parametric finite-volume theory for functionally graded materials. Journal of Computational Materials Science 2008; 44(2): 422-438.

[13] Cavalcante M A A, Marques S P C, Pindera M J. Transient thermo-mechanical analysis of a layered cylinder by the parametric finite-volume theory. Journal of Thermal Stresses 2009; 32(1): 112-134.

[14] Tanigawa Y, Ootao Y. Transient piezothermoelasticity of a two-layered composite hollow cylinder constructed of isotropic elastic and piezoelectric layers due to asymmetrical heating. Journal of Thermal Stresses 2007; 30(8): 1003-1023.

[15] Chatzigeorgiou G, Kalpakides V, Charalambakis N. Biaxial loading of continuously graded thermoviscoplastic materials. Computational Mechanics 2007; 39(4): 335-355.

[16] Cavalcante M A A, Marques S P C, Pindera M J. Parametric formulation of the finite-volume theory for functionally graded materials Part II: numerical results. Journal of Applied Mechanics 2007; 74(5): 946-957.

Biography:

Sun Zhigang Born in 1976, he received B.S. and M.S. degrees from Nanjing University of Aeronautics and Astronautics in 2002 and 2005 respectively, and then became a teacher there. His main research interest is aerospace propulsion theory and engineering.
E-mail: szg_mail@nuaa.edu.cn